https://doi.org/10.5194/egusphere-2026-5978
Preprint. Discussion started: 12 November 2026
© Author(s) 2026. CC BY 4.0 License.

Brief communication: Tidal timing and minutes to act during the 15 August 2026 Flores tsunami

Arya Iwantoro[1], Rima Harahap[1,2], Sarah Boulton[3], Gerd Masselink[1]

[1]Centre for Coastal and Ocean Processes and Engineering (C-COPE), University of Plymouth, Plymouth, PL4 8AA, UK
[2]Ocean Engineering Department, Kalimantan Institute of Technology, Balikpapan, 76127, Indonesia
[3]Centre for Research in Natural Hazards and Risk Reduction (CHaRR), University of Plymouth, Plymouth, PL4 8AA, UK

Correspondence to: Arya Iwantoro (arya.iwantoro@plymouth.ac.uk)

Abstract. The 15 August 2026 Flores tsunami provides a case for evaluating how tidal timing can alter inundation. We reconstruct the event with coupled Delft3D-SFINCS simulations constrained by post-event observations. We then simulate the same tsunami at high tide (+0.7 m relative to mean sea level, MSL), representing the spring high tide recorded on the event day. Relative to the 3.81 km^2 reconstructed-event inundation above highest astronomical tide (HAT), high tide increases inundated area to 11.84 km^2, a 3.1-fold increase. These results support tide-informed hazard maps, evacuation planning, community education, and preparedness close to tsunami sources.

1 Introduction

On 15 August 2026, a major earthquake on the Flores Back-Arc Thrust generated a tsunami along the northern coast of Flores. The Flores region of eastern Indonesia lies within an active island-arc and back-arc setting exposed to tsunami hazard from local offshore earthquakes and regional sources, and the Flores Back-Arc Thrust is a major local source capable of affecting nearby coasts within minutes (Pranantyo et al., 2021; Felix et al., 2022). The destructive 12 December 1992 Flores tsunami remains the clearest historical reminder of this hazard, causing severe coastal damage and more than 2000 fatalities, with tsunami arrival reported within only a few minutes after the earthquake at some locations (Yeh et al., 1993; Lander et al., 2003; Hidayat et al., 1995). Field and modelling studies of the 1992 event also showed strong spatial variability in run-up and inundation, influenced by bathymetry, coastal geometry, and possible submarine slope failures (Hidayat et al., 1995; Lander et al., 2003).

The 2026 event is treated here as a near-field tsunami because its source was close to the affected northern coast of Flores, leaving only a short warning and response time (Rahayu et al., 2026a, b; USGS, 2017). BMKG issued a tsunami early warning 2 min 16 s after the main shock and reported tsunami signals at multiple tide gauges, including Reo and Pota (Fig. 1a), where wave heights were about 1.6 m (Rahayu et al., 2026a, b). BMKG field surveys recorded the highest run-up at Desa Salama (2.68 m) and the farthest inundation distance at Nampar Sepang (145 m) (Rahayu et al., 2026a). The tsunami damaged 23 houses, including two swept away at Desa Salama, but BMKG reported no fatalities after communities evacuated following

https://doi.org/10.5194/egusphere-2026-5978
Preprint. Discussion started: 12 November 2026
© Author(s) 2026. CC BY 4.0 License.

the warning (Rahayu et al., 2026a). The event therefore provides a useful recent case for examining how tidal timing and higher baseline water levels could change tsunami inundation when coastal communities may have only minutes to respond.

Tide stage is important during tsunami events because the same tsunami wave can produce different inundation depths and extents depending on the water level at arrival. The tide reconstruction indicates that the 15 August 2026 tsunami reached the coast close to mean sea level, at approximately -0.08 m relative to MSL, providing an opportunity to examine how the impact might have changed if the waves had arrived at high tide. Here, we use a coupled Delft3D-SFINCS modelling framework to reconstruct the observed event and compare it with a high-tide scenario of +0.7 m relative to MSL, corresponding to the highest predicted tide on the day of the event and slightly above the local mean high-water springs level at Reo. The observed-tide simulation was constrained by the Indonesian Geospatial Information Agency (BIG) tide-gauge observations (BIG, 2026a) and evaluated against BMKG field-survey tsunami heights (Rahayu et al., 2026a). We also use a high-tide plus 2100 sea-level-rise case to indicate how the future run-up limit could change under higher sea level. We ask two questions: (1) how much does high tide increase inundation area, mean inundation depth, and maximum run-up under the same tsunami forcing, and (2) what do these results imply for hazard mapping, evacuation planning, community education, and near-field tsunami early warning?

2 Data and methods

2.1 Event, observations, and tide condition

The 15 August 2026 Flores tsunami was generated by a shallow thrust earthquake north of Flores, associated with the Flores Back-Arc Thrust. The USGS finite-fault solution gives a magnitude of Mw 7.76, while BMKG reported a focal depth of approximately 15 km and an epicentre about 30 km northeast of Nagekeo (Rahayu et al., 2026b; USGS, 2017). Post-event field observations and tsunami-gauge records were taken from BMKG reports and include run-up, inundation distance, damage, and recorded tsunami wave heights at affected locations along the north coast of Flores (Rahayu et al., 2026a, b). These records provide the main observational constraints on the regional tsunami signal. The surveyed locations and tide-gauge stations are shown in Fig. 1a.

The tide condition at tsunami arrival was estimated from tide-gauge records from the BIG tide-gauge station at Reo, as reported in the BMKG reports (BIG, 2026a; Rahayu et al., 2026b). The record indicates that the tsunami reached the coast at approximately -0.08 m relative to MSL as shown in Fig. 1b. This tide estimate is used to define the observed event water level, while the BMKG observations are used in the model-data comparison reported in Appendix B.

2.2 Model setup

We adopted a Delft3D-SFINCS modelling chain, with Delft3D-FLOW version 4.03.01 resolving offshore tsunami propagation and SFINCS simulating nearshore inundation. SFINCS is a reduced-physics coastal-flooding model (Leijnse et al., 2021), and

https://doi.org/10.5194/egusphere-2026-5978
Preprint. Discussion started: 12 November 2026
© Author(s) 2026. CC BY 4.0 License.

coupled Delft3D-SFINCS workflows have been applied to tsunami inundation modelling for Tōhoku tsunami in Japan (Röbke et al., 2021). The tsunami source was based on the USGS finite-fault solution for event us6000tkt2 and converted to initial sea-surface deformation using Delft Dashboard (Okada, 1985; van Ormondt et al., 2020). Offshore bathymetry, nearshore bathymetry, and land elevation were taken from BATNAS, Allen Coral Atlas, and DeltaDTM, respectively (Allen Coral Atlas, 2022; BIG, 2026b; Pronk et al., 2024). Full model-domain and input-data details are provided in Appendix A.

2.3 Model scenarios

Two main water-level scenarios were simulated with the modelling chain. The first is the observed-tide scenario, which represents the reconstructed tide level at the time of tsunami arrival, approximately -0.08 m relative to mean sea level (MSL). This scenario was evaluated against BMKG tsunami-gauge and field-survey observations before being used as the basis for comparison. The second is the high-tide scenario, in which the same Delft3D-FLOW tsunami forcing was applied in SFINCS, but with the still-water level set to +0.7 m relative to MSL. This level corresponds to the highest predicted tide on the day of the event and is slightly above the local mean high water springs level at Reo (+0.65 m relative to MSL) (BIG, 2026a). As a supporting future-water-level case, we also simulated high tide plus 0.81 m of sea-level rise, representing the SSP5-8.5 50th percentile projection for 2100 (Garner et al., 2021). This case is used only to map the future run-up limit, because the still-water baseline is shifted by the sea-level-rise offset and its inundated area is not directly comparable with the present-day observed-tide and high-tide scenarios. All other model settings, including the tsunami source, bathymetry, topography, and numerical grid, were kept unchanged, so the comparison between the two main scenarios isolates the effect of tidal timing on inundation depth and extent.

https://doi.org/10.5194/egusphere-2026-5978
Preprint. Discussion started: 12 November 2026
© Author(s) 2026. CC BY 4.0 License.

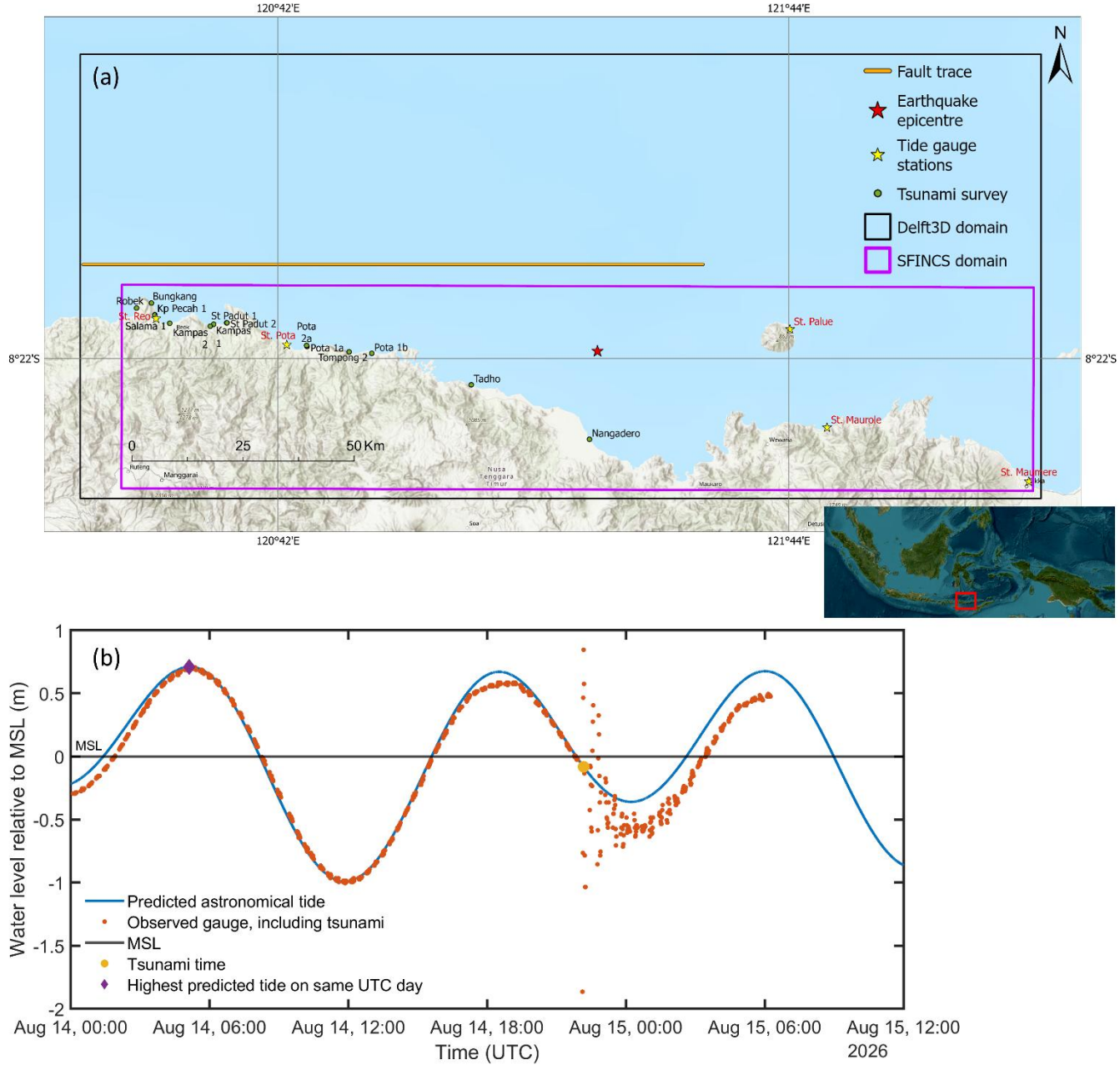


Figure 1: Study area and its water level conditions during the 15 August 2026 Flores tsunami showing (a) Delft3D and SFINCS model domain, showing the earthquake location, fault trace according to USGS (2017), tide-gauge stations (BIG, 2026a), and BMKG tsunami-survey locations (Rahayu et al., 2026a) with the inset map shows the regional location of Flores within Indonesia; and (b) BIG's tide-gauge water-level record (red dot) and predicted astronomical tide (solid blue line) from 14–15 August 2026 at Reo. Water levels are shown in metres relative to mean sea level (MSL). The observed gauge record includes the tsunami signal. The yellow marker indicates the tsunami time, and the purple marker indicates the highest predicted tide on the same UTC day. Basemap sources: Geosciences Australia, Esri, GEBCO, Garmin, NaturalVue, TomTom, FAO, METI/NASA, and USGS | Powered by ESRI.

https://doi.org/10.5194/egusphere-2026-5978
Preprint. Discussion started: 12 November 2026
© Author(s) 2026. CC BY 4.0 License.

3 Results

The reconstructed observed-tide simulation inundates 3.81 km2 above present-day highest astronomical tide (HAT) along the north coast of Flores (Fig. 2). Under the same tsunami forcing, the high-tide scenario increases the inundated area above HAT to 11.84 km^2, corresponding to a 3.1-fold increase. The spatial pattern in Fig. 2 shows that this increase is not distributed uniformly along the coast. Instead, inundation expands mainly around low-lying coastal plains and embayed shoreline sections, while narrower or steeper coastal settings show more limited landward expansion.

The site-scale metrics in Fig. 3 quantify this spatial pattern. Across the ten analysed locations, high tide increases inundated area by 0.05-1.47 km^2, mean inundation depth by 0.08-0.29 m, and maximum run-up by 0.15-0.81 m. The largest increases in inundated area occur at Mbay II, Marapokot, Lengkosambi, Aerama, and Mata Air-Salama, where wider low-lying coastal plains allow flooding to expand inland (Fig. 3a). In contrast, sites such as Wangkung and Tadho show smaller increases in inundated area, even though mean inundation depth and run-up still increase (Fig. 3b, c). High tide increases inundated area, mean depth, and run-up at all analysed locations, but the magnitude of change varies among sites. This variability is greatest for inundated area, which depends strongly on the width and elevation of the coastal plain behind the shoreline.

The high-tide plus sea-level-rise case is shown in Fig. 2 only as a future run-up-limit line. This case indicates where a higher future still-water level could shift the potential landward limit of tsunami impact, but it is not treated as a directly comparable inundation-area scenario because the baseline water level differs from the present-day observed-tide and high-tide scenarios.

https://doi.org/10.5194/egusphere-2026-5978
Preprint. Discussion started: 12 November 2026
© Author(s) 2026. CC BY 4.0 License.

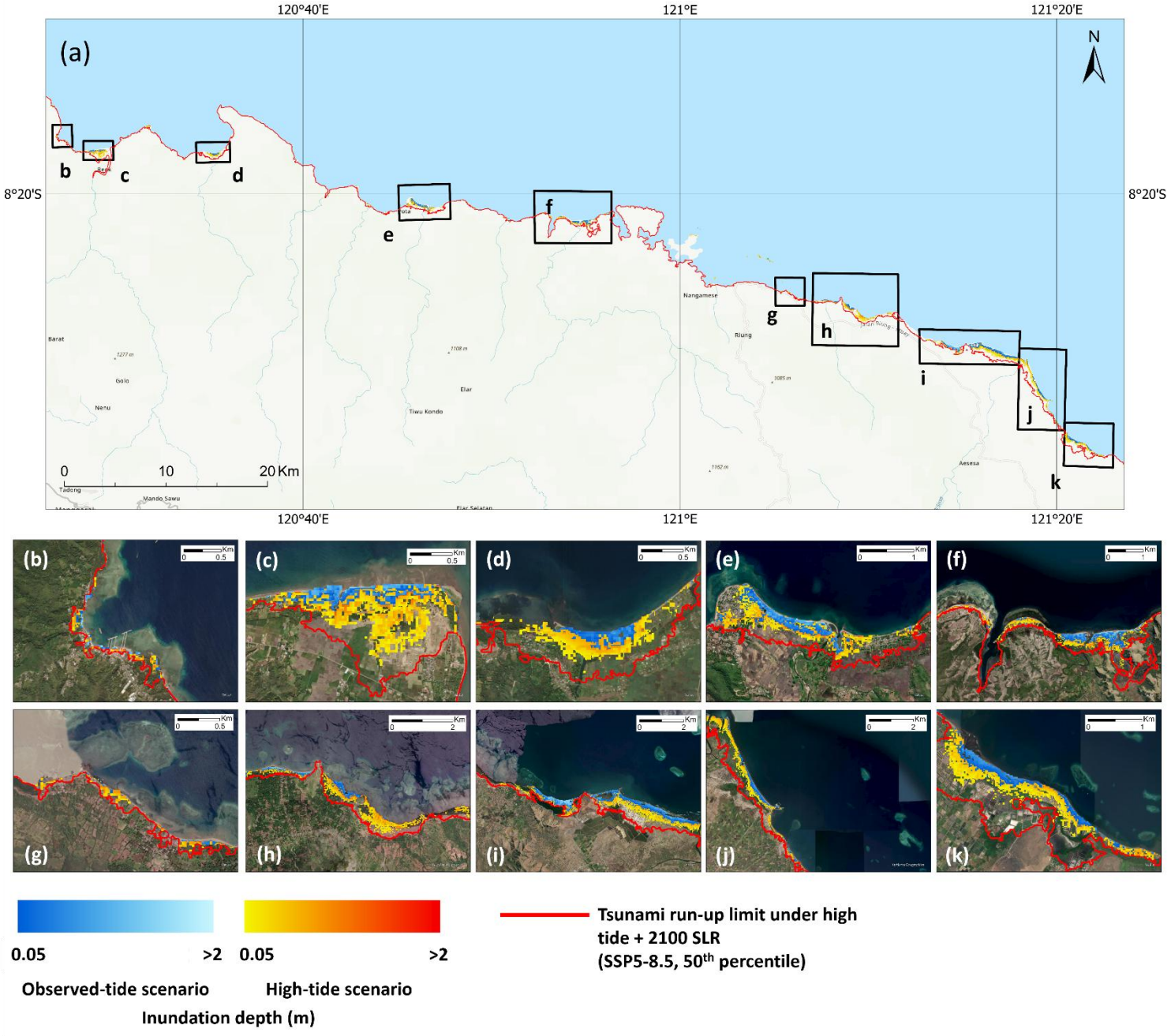


Figure 2: Comparison of simulated maximum tsunami inundation depth under the observed-tide and high-tide scenarios along the northern Flores coastline. Panel (a) shows the regional distribution of inundation above present-day highest astronomical tide (HAT), selected coastal areas, and the high-tide plus 2100 sea-level-rise run-up limit. Detailed panels show populated and strongly affected coastal areas selected for site-scale comparison: (b) Wangkung, (c) Mata Air-Salama, (d) Padut-Kampas, (e) Pota, (f) Golo Lijun, (g) Tadho, (h) Lengkosambi, (i) Mbay II, (j) Marapokot, and (k) Aerama. Blue shades show the observed-tide scenario, yellow-red shades show the high-tide scenario, and the red line indicates the projected run-up limit under high tide plus 2100 sea-level rise. Basemap credits: Esri, TomTom, Garmin, METI/NASA, and USGS | Powered by ESRI.

https://doi.org/10.5194/egusphere-2026-5978
Preprint. Discussion started: 12 November 2026
© Author(s) 2026. CC BY 4.0 License.

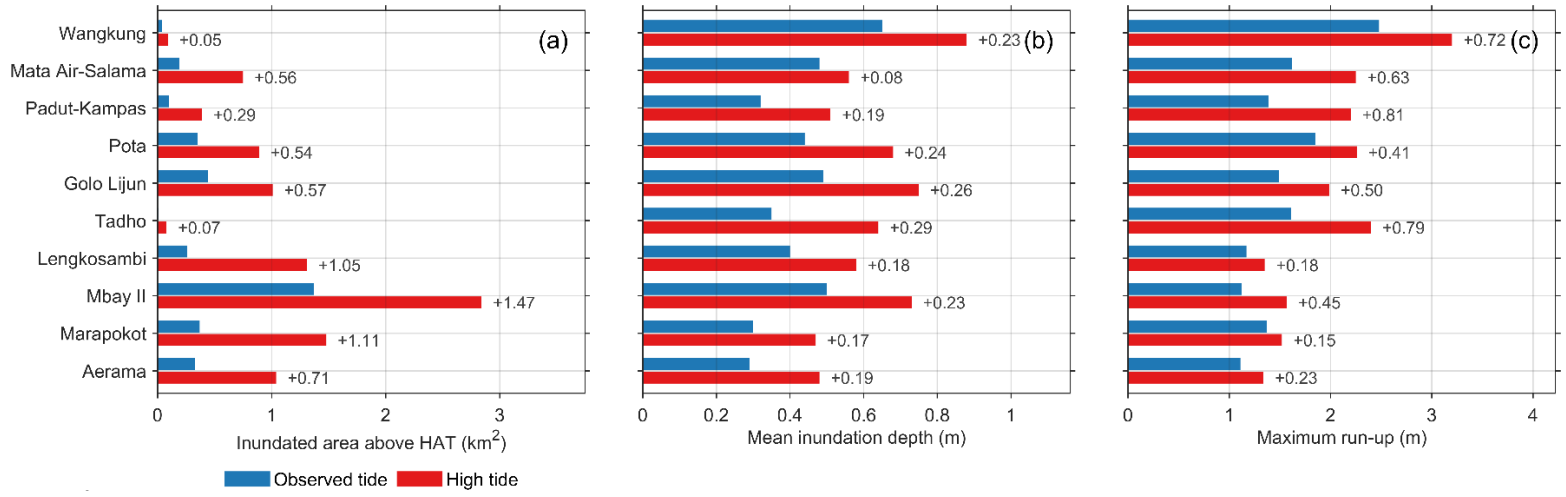


Figure 3. Site-scale comparison of simulated tsunami impact metrics under the observed-tide and high-tide scenarios at the populated and strongly affected coastal areas from west to east as shown in Fig. 2b-k, showing (a) inundated area above present-day highest astronomical tide (HAT), (b) mean inundation depth, and (c) maximum run-up. Blue bars show the observed-tide scenario, red bars show the high-tide scenario, and labels indicate the increase under high tide.

4 Discussion and conclusions

The inundation pattern is spatially variable, with larger flooded areas around coastal plains and embayed sections of the shoreline rather than a continuous inundation belt along the whole coast. This pattern is consistent with the BMKG post-event survey, which reported localised run-up and inundation impacts at surveyed sites rather than uniform flooding along the coastline (Rahayu et al., 2026a). The model-data comparison in Appendix B shows that the observed-tide simulation reproduces the broad spatial pattern of the surveyed tsunami heights, while retaining local discrepancies expected in complex coastal settings. The site-scale comparison shows that high tide increases inundated area, mean inundation depth, and run-up at all analysed locations, but the magnitude of change varies among sites, especially for inundated area, which depends on the width and geomorphological landscape of the coastal plain behind the shoreline.

The scenario comparison shows that tidal timing was an important control on the coastal impact of the 15 August 2026 Flores tsunami. This result is consistent with previous studies showing that tide stage and background sea level can substantially affect tsunami water levels, inundation depths, and inundation extents (Mofjeld et al., 2007; Adams et al., 2015). In this case, the high-tide scenario produced substantially wider inundation under the same tsunami forcing, showing that a different tidal arrival time could have changed the realised coastal impact. The supporting high-tide plus SLR case further indicates that

https://doi.org/10.5194/egusphere-2026-5978
Preprint. Discussion started: 12 November 2026
© Author(s) 2026. CC BY 4.0 License.

higher future still-water levels could shift the potential run-up limit inland, although it is not used here as a directly comparable inundation-area scenario.

From a disaster-management perspective, the 2026 event should be framed carefully. It was not a repeat of the destructive 1992 Flores tsunami, because the tsunami was smaller and arrived close to mean sea level. The limited observed inundation should therefore not be interpreted as evidence of low tsunami hazard. Instead, it shows that realised impact can depend strongly on timing. BMKG's rapid warning and post-event survey provide essential evidence for learning from the tsunami, while our modelling shows that a similar event arriving at high tide could produce substantially wider flooding. Official warning systems remain essential, but should be complemented by hazard maps, evacuation planning, and community education that help coastal communities act within minutes. These priorities are consistent with UNESCO-IOC Tsunami Ready guidance, which emphasises evacuation maps, public awareness, education activities, signage, and community exercises (UNESCO-IOC, 2022).

The results support three practical implications for tsunami risk reduction in Flores and comparable island settings. First, tsunami hazard maps should account for tidal stage, because the same tsunami forcing can produce substantially different inundation extents depending on the water level at arrival. Second, BMKG's established practice of combining post-event surveys with rapid numerical modelling should be maintained and extended by documenting the tidal level at tsunami arrival and, where feasible, testing a range of tidal conditions. Field observations constrain event size and model performance, while numerical simulations translate these constraints into spatial inundation information. Third, community education and evacuation planning should emphasise that a limited observed impact does not represent the full plausible hazard, particularly if a future tsunami of similar or greater magnitude arrives at high tide. Future sea-level rise should also be considered when hazard maps are updated, because it may shift the potential run-up limit farther inland.

The analysis is designed to isolate the effect of tidal timing by holding the tsunami forcing, bathymetry, topography, and numerical settings constant between the observed-tide and high-tide scenarios. It is therefore not a probabilistic hazard assessment and does not represent the full range of possible earthquake sources or compound water-level conditions. Instead, it shows how strongly inundation can change for the same tsunami when the arrival tide differs.

In conclusion, the 15 August 2026 Flores tsunami provides a timely case for rapid, observation-constrained tsunami inundation modelling. The Delft3D-SFINCS reconstruction reproduces the observed order of magnitude of tsunami heights, while the scenario comparison shows that high tide increases inundated area above HAT from 3.81 to 11.84 km^2 under the same tsunami forcing. This 3.1-fold increase shows that tidal timing can strongly influence tsunami impact. The response also varies among coastal settings, with the largest area increases where low-lying coastal plains allow flooding to expand inland. These findings strengthen the case for tide-informed hazard mapping, evacuation planning, coastal community education, and near-field tsunami preparedness that combines official warning with immediate self-evacuation capacity.

https://doi.org/10.5194/egusphere-2026-5978
Preprint. Discussion started: 12 November 2026
© Author(s) 2026. CC BY 4.0 License.

Appendix A: Model setup

The tsunami source parameters, model domains, grid settings, and main topographic-bathymetric inputs are summarised in Table A1. The Delft3D-FLOW domain covers approximately 215 km × 100 km along the northern Flores region, with a structured grid of 1082 × 502 cells and a horizontal grid resolution of approximately 200 m. The SFINCS domain covers approximately 203 km × 45 km, with a grid of 5083 × 1125 cells, a horizontal resolution of 40 m, and a 10 m subgrid representation for the coastal inundation calculations. Delft3D-FLOW was run for 1 h from the earthquake time, and the resulting tsunami water-level signal was transferred to the SFINCS domain. Maximum inundation depth was defined as the highest simulated water depth over land above present-day highest astronomical tide (HAT), while inundation extent was calculated as the total flooded area above present-day HAT. This HAT-based definition avoids counting areas that are already within the present-day upper tidal zone as tsunami inundation.

https://doi.org/10.5194/egusphere-2026-5978
Preprint. Discussion started: 12 November 2026
© Author(s) 2026. CC BY 4.0 License.

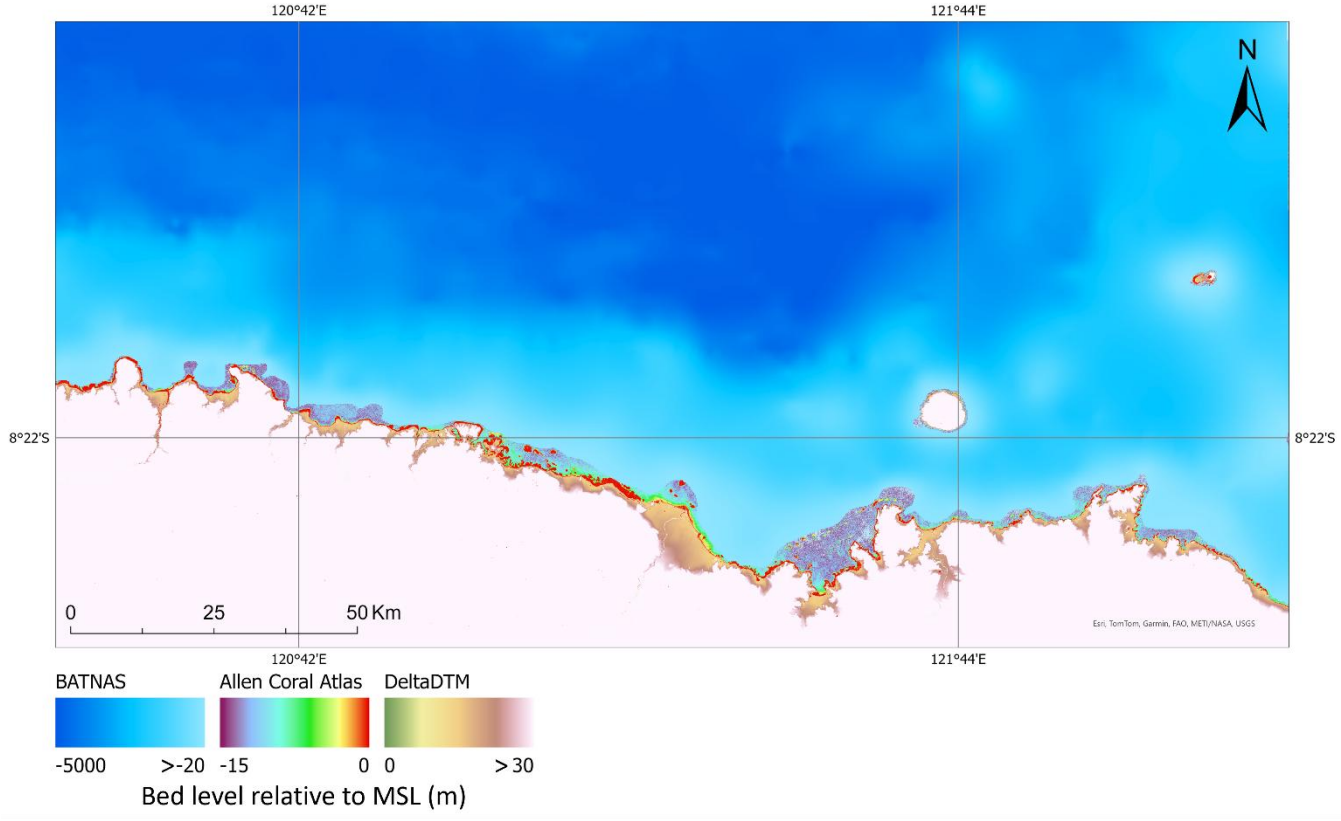
Table A1. Tsunami source, model-domain, and topographic-bathymetric parameters used in the Delft3D-FLOW and SFINCS simulations.

Model	Parameter		Unit	Value	Source and method
Tsunami source	M_w	Moment magnitude of the earthquake source	–	7.76	USGS (2017)
	Φ	Fault strike angle; orientation of the fault trace measured clockwise from north	°	90	
	d	Fault depth below the surface	km	10	
	Δ	Fault dip angle; inclination of the fault plane from the horizontal	°	32	
	λ	Fault rake angle; direction of slip on the fault plane relative to strike	°	90	
	L	Fault length; along-strike dimension of the rupture	km	138.2	Okada (1985); van Ormondt et al. (2020)
	W	Fault width; down-dip dimension of the rupture	km	49.5	
	D	Fault slip; relative displacement across the fault during rupture	m	2.4	USGS (2017)
Delft3D	Δx	Horizontal computational grid spacing in the x-direction	m	200	best estimate
	Δy	Horizontal computational grid spacing in the y-direction	m	200	best estimate
	Δt	Computational time step	s	3	best estimate
	N	Manning bottom-roughness coefficient used to parameterise bed friction	$s\ m^{-1/3}$	0.02	best estimate
SFINCS	ν_h	Horizontal eddy-viscosity coefficient controlling horizontal momentum diffusion	$m^2\ s^{-1}$	1	best estimate
	Δx	Horizontal computational grid spacing in the x-direction	m	40	best estimate
	Δy	Horizontal computational grid spacing in the y-direction	m	40	best estimate
	Δx_{sg}	Subgrid resolution used for high-resolution bathymetry and topography	m	10	best estimate
	Δt	Computational time step	s	3	best estimate
	α	CFL-based time-step reduction factor used for numerical stability	–	0.5	Gaido-Lasserre et al. (2024)
	ϑ	Numerical weighting / smoothing parameter used in the momentum scheme	–	0.9	Best estimate
	n	Default Manning roughness coefficient	$s\ m^{-1/3}$	0.04	Gaido-Lasserre et al. (2024)
	n_{land}	Manning roughness coefficient applied to land areas	$s\ m^{-1/3}$	0.035	
	n_{sea}	Manning roughness coefficient applied to sea areas	$s\ m^{-1/3}$	0.02	

The topographic and bathymetric data were assembled from multiple sources to represent offshore propagation, nearshore transformation, and land inundation (Fig. S1). BATNAS national bathymetry, with a resolution of approximately 180 m, was used for offshore bathymetry in water depths deeper than about 20 m (BIG, 2026b). Nearshore reef and shallow-water bathymetry were represented using the Allen Coral Atlas at approximately 10 m resolution for water depths of 0-15 m (Allen Coral Atlas, 2022). For land elevations, we used a Deltares digital terrain model (DeltaDTM) with approximately 30 m

https://doi.org/10.5194/egusphere-2026-5978
Preprint. Discussion started: 12 November 2026
© Author(s) 2026. CC BY 4.0 License.

resolution from Pronk et al. (2024). These datasets were merged to construct the Delft3D-FLOW bathymetry and the SFINCS subgrid topography-bathymetry used for inundation modelling.



195 **Figure A1. Topographic and bathymetric datasets used to construct the model bed level relative to mean sea level. BATNAS represents offshore bathymetry, the Allen Coral Atlas represents nearshore reef and shallow-water bathymetry, and DeltaDTM represents land elevation. Basemap sources: Esri, Garmin, TomTom, NGA, FAO, METI/NASA, and USGS | Powered by ESRI.**

Appendix B: Model evaluation

The observed-tide simulation was evaluated against BMKG field-survey observations of maximum tsunami height at 19 paired
200 locations (Fig. B1) and available tide-gauge records. The comparison gives a root-mean-square error (RMSE) of 0.52 m, a coefficient of determination (R^2) of 0.46, and a mean bias of -0.033 m, calculated as modelled minus observed height. These statistics show that the model reproduces the observed order of magnitude and broad spatial trend of tsunami height, with limited overall bias, but that scatter remains at individual sites. This scatter is expected for a rapid regional inundation model in this coastal setting. The affected shoreline includes complex beach morphology, estuary mouths, tidal channels, nearshore
205 bathymetric gradients, houses, and coastal infrastructure. These features can steer shallow flow over short distances and create

https://doi.org/10.5194/egusphere-2026-5978
Preprint. Discussion started: 12 November 2026
© Author(s) 2026. CC BY 4.0 License.

local flow structures that are not fully resolved by the 40 m model grid and 10 m subgrid representation. The validation is therefore used as an order-of-magnitude check on the reference inundation pattern, rather than as evidence that the model resolves every local flow pathway.

The model results are also broadly consistent with the BMKG report and press release for the same event. BMKG reported modelled tsunami heights of approximately 0.5-2.0 m along affected parts of northern Flores and localised inundation at several populated coastal areas (Rahayu et al., 2026a, b). The SFINCS simulation similarly produces tsunami heights within the observed range and localised inundation along the affected northern Flores coastline. This agreement supports using the observed-tide simulation as the basis for comparing the observed-tide and high-tide scenarios, while recognising that source uncertainty, bathymetric uncertainty, and unresolved site-scale flow controls may affect individual locations. The high-tide plus SLR case is therefore used only to illustrate the potential future run-up limit.

https://doi.org/10.5194/egusphere-2026-5978
Preprint. Discussion started: 12 November 2026
© Author(s) 2026. CC BY 4.0 License.

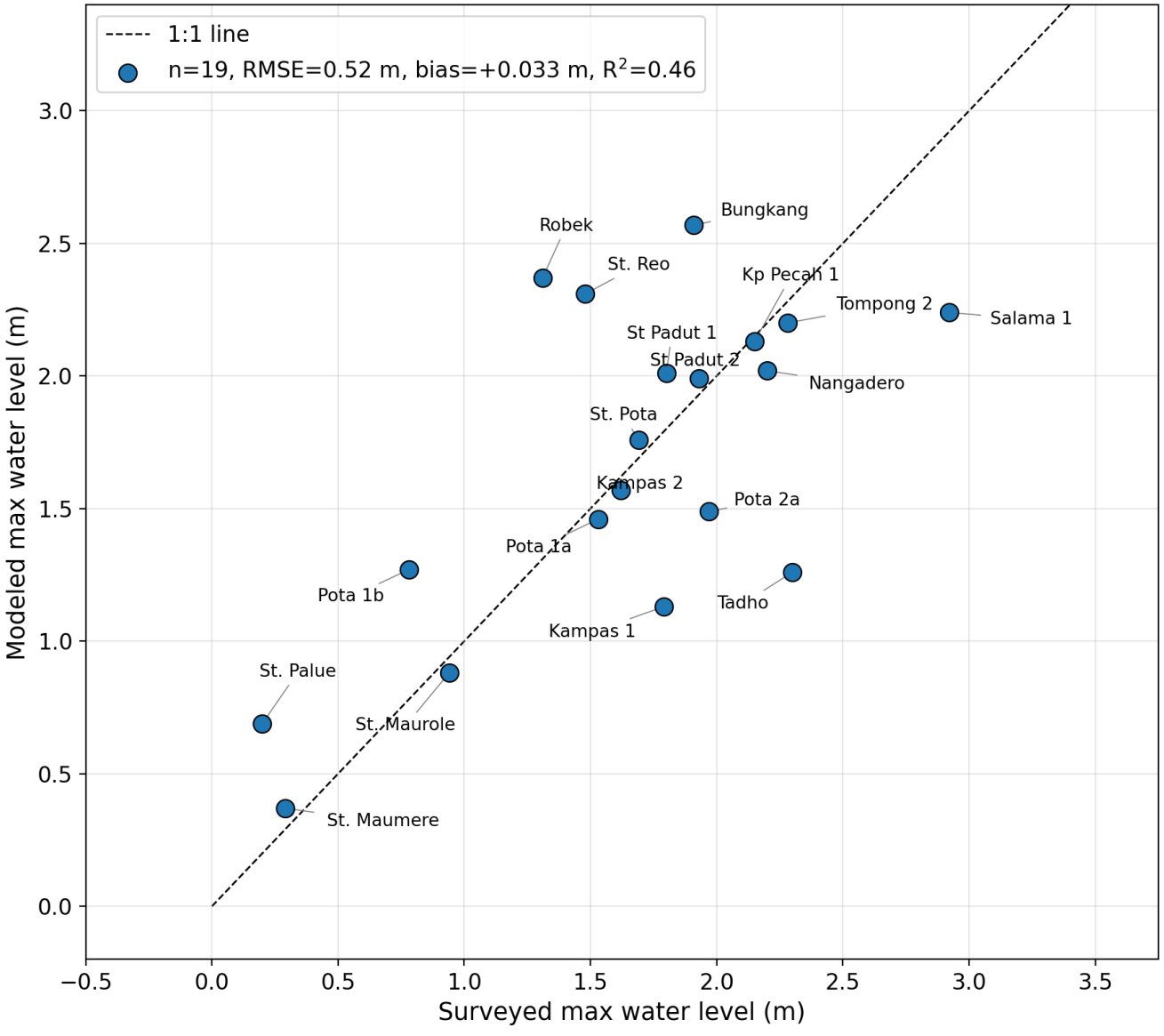


Figure B1. Surveyed and modelled maximum tsunami heights at the 19 BMKG field-survey locations. The dashed line marks the 1:1 relation. The survey locations are shown in Fig. 1 of the main manuscript.

Code and data availability

The model configuration files, processed model inputs, observation–model comparison data, and maximum-inundation outputs generated in this study will be archived in Zenodo prior to final publication. The third-party datasets used in this study are publicly available from their original providers. BMKG tide-gauge observations, post-event field-survey observations, and the

https://doi.org/10.5194/egusphere-2026-5978
Preprint. Discussion started: 12 November 2026
© Author(s) 2026. CC BY 4.0 License.

BMKG numerical modelling report used for model evaluation are available from BMKG at https://www.bmkg.go.id/artikel/jejak-tsunami-flores-15-agustus-2026 and https://www.bmkg.go.id/artikel/model-numerik-tsunami-flores-2026. Additional tide-gauge observations at Reo were obtained from the Indonesian Geospatial Information Agency (BIG) through the Sistem Referensi Geospasial Indonesia (SRGI) at https://srgi.big.go.id/tides/PREO. The finite-fault source used to initialise the tsunami simulation was obtained from the USGS event page for event ID us6000tkt2 at https://earthquake.usgs.gov/earthquakes/eventpage/us6000tkt2/finite-fault. Offshore bathymetry was obtained from the Indonesian National Bathymetry dataset (BATNAS), provided by BIG through Ina-Geoportal at https://tanahair.indonesia.go.id/portal-web/. Nearshore reef and shallow-water bathymetry were derived from the Allen Coral Atlas, available at https://doi.org/10.5281/zenodo.3833242. Topographic elevation data were obtained from DeltaDTM (https://doi.org/10.1038/s41597-024-03091-9).

Author contributions

API contributed to conceptualization, supervision, writing the original draft, and reviewing and editing the manuscript. RH contributed to conceptualization, data curation, formal analysis, funding acquisition, investigation, methodology, validation, and visualization. SJB contributed to conceptualization, supervision, and reviewing and editing the manuscript. GM contributed to conceptualization, supervision, project administration, and reviewing and editing the manuscript. All authors reviewed and approved the final manuscript.

Competing interests

The authors declare that they have no conflict of interest.

Acknowledgements

The authors thank the BMKG and BIG for making its tide-gauge records, post-event field-survey observations, and numerical tsunami-modelling report publicly available.

Financial support

This research has been supported by the Indonesia Endowment Fund for Education (Lembaga Pengelola Dana Pendidikan, LPDP), Ministry of Finance of the Republic of Indonesia (award no. 202302220210684, awarded to Rima Harahap).

https://doi.org/10.5194/egusphere-2026-5978
Preprint. Discussion started: 12 November 2026
© Author(s) 2026. CC BY 4.0 License.

References

Adams, L. M., LeVeque, R. J., and González, F. I.: The Pattern Method for incorporating tidal uncertainty into probabilistic tsunami hazard assessment (PTHA), Natural Hazards, 76, 19-39, https://doi.org/10.1007/s11069-014-1482-z, 2015.

Allen Coral Atlas: Imagery, maps and monitoring of the world's tropical coral reefs, Allen Coral Atlas [dataset], https://doi.org/10.5281/zenodo.3833242, 2022.

BIG: SRGI tide station PREO, Badan Informasi Geospasial [dataset], https://srgi.big.go.id/tides/PREO, 2026a.

BIG: BATNAS - Batimetri Nasional, Badan Informasi Geospasial [dataset], https://tanahair.indonesia.go.id/portal-web/, 2026b.

Felix, R. P., Hubbard, J. A., Bradley, K. E., Lythgoe, K. H., Li, L., and Switzer, A. D.: Tsunami hazard in Lombok and Bali, Indonesia, due to the Flores back-arc thrust, Nat. Hazards Earth Syst. Sci., 22, 1665-1682, https://doi.org/10.5194/nhess-22-1665-2022, 2022.

Gaido-Lasserre, C., Nederhoff, K., Storlazzi, C. D., Reguero, B. G., and Beck, M. W.: Improved efficient physics-based computational modeling of regional wave-driven coastal flooding for reef-lined coastlines, Ocean Modelling, 189, 102358, https://doi.org/10.1016/j.ocemod.2024.102358, 2024.

Garner, G. G., Hermans, T., Kopp, R. E., Slangen, A. B. A., Edwards, T. L., Levermann, A., Nowicki, S., Palmer, M. D., Smith, C., Fox-Kemper, B., Hewitt, H. T., Xiao, C., Aðalgeirsdóttir, G., Drijfhout, S. S., Golledge, N. R., Hemer, M., Krinner, G., Mix, A., Notz, D., Nurhati, I. S., Ruiz, L., Sallée, J. B., Yu, Y., Hua, L., Palmer, T., and Pearson, B.: IPCC AR6 Sea Level Projections (20210809), Zenodo [dataset], https://doi.org/10.5281/zenodo.5914709, 2021.

Hidayat, D., Barker, J. S., and Satake, K.: Modeling the seismic source and tsunami generation of the December 12, 1992 Flores Island, Indonesia, earthquake, pure and applied geophysics, 144, 537-554, https://doi.org/10.1007/BF00874382, 1995.

Lander, J. F., Whiteside, L. S., and Lockridge, P. A.: Two decades of global tsunamis, Science of Tsunami Hazards, 21, 3, https://doaj.org/article/b701c4038bcd4b4f852bd382cbeeae71, 2003.

Leijnse, T., van Ormondt, M., Nederhoff, K., and van Dongeren, A.: Modeling compound flooding in coastal systems using a computationally efficient reduced-physics solver: Including fluvial, pluvial, tidal, wind- and wave-driven processes, Coastal Engineering, 163, 103796, https://doi.org/10.1016/j.coastaleng.2020.103796, 2021.

Mofjeld, H. O., González, F. I., Titov, V. V., Venturato, A. J., and Newman, J. C.: Effects of Tides on Maximum Tsunami Wave Heights: Probability Distributions, Journal of Atmospheric and Oceanic Technology, 24, 117-123, https://doi.org/10.1175/JTECH1955.1, 2007.

Okada, Y.: Surface deformation due to shear and tensile faults in a half-space, Bulletin of the Seismological Society of America, 75, 1135-1154, https://doi.org/10.1785/BSSA0750041135, 1985.

Pranantyo, I. R., Heidarzadeh, M., and Cummins, P. R.: Complex tsunami hazards in eastern Indonesia from seismic and non-seismic sources: Deterministic modelling based on historical and modern data, Geoscience Letters, 8, 20, https://doi.org/10.1186/s40562-021-00190-y, 2021.

https://doi.org/10.5194/egusphere-2026-5978
Preprint. Discussion started: 12 November 2026
© Author(s) 2026. CC BY 4.0 License.

Pronk, M., Hooijer, A., Eilander, D., Haag, A., de Jong, T., Vousdoukas, M., Vernimmen, R., Ledoux, H., and Eleveld, M.: DeltaDTM: A global coastal digital terrain model, Scientific Data, 11, 273, https://doi.org/10.1038/s41597-024-03091-9, 2024.

Rahayu, T., Wijayanto, Pribadi, S., Gunawan, I., Fauzi, Riama, N. F., Fathani, T. F., Harva, M., Waliya, A., and Tim, S.: Jejak Tsunami Flores 15 Agustus 2026 di Manggarai, https://www.bmkg.go.id/artikel/jejak-tsunami-flores-15-agustus-2026, 2026a.

Rahayu, T., Pribadi, S., Fathani, T. F., Harvan, M., Pandadaran, S. H., Haryanto, F. T., Gunawan, I., Fauzi, Handayani, T., Waliya, A., and Zhofiro, F. N.: Model Numerik Tsunami Flores 2026, Badan Meteorologi, Klimatologi, dan Geofisika, Jakarta, https://www.bmkg.go.id/artikel/model-numerik-tsunami-flores-2026, 2026b.

Röbke, B. R., Leijnse, T., Winter, G., van Ormondt, M., van Nieuwkoop, J., and de Graaff, R.: Rapid Assessment of Tsunami Offshore Propagation and Inundation with D-FLOW Flexible Mesh and SFINCS for the 2011 Tōhoku Tsunami in Japan, https://doi.org/10.3390/jmse9050453, 2021.

UNESCO-IOC: Standard guidelines for the Tsunami Ready Recognition Programme, IOC. Manuals and guides, UNESCO/IOC, 62 pages pp., https://doi.org/10.25607/OBP-1845, 2022.

USGS: Advanced National Seismic System (ANSS) Comprehensive Catalog of Earthquake Events and Products, U.S. Geological Survey [dataset], https://doi.org/10.5066/F7MS3QZH, 2017.

van Ormondt, M., Nederhoff, K., and van Dongeren, A.: Delft Dashboard: a quick set-up tool for hydrodynamic models, Journal of Hydroinformatics, 22, 510-527, https://doi.org/10.2166/hydro.2020.092, 2020.

Yeh, H., Imamura, F., Synolakis, C., Tsuji, Y., Liu, P., and Shi, S.: The Flores Island tsunamis, Eos, Transactions American Geophysical Union, 74, 369-373, https://doi.org/10.1029/93EO00381, 1993.